

Leveraging power grid topology in machine learning assisted optimal power flow

Thomas Falconer and Letif Mones

Abstract—Machine learning assisted optimal power flow (OPF) aims to reduce the computational complexity of these non-linear and non-convex constrained optimisation problems by consigning expensive (online) optimisation to offline training. The majority of work in this area typically employs fully-connected neural networks (FCNN). However, recently convolutional (CNN) and graph (GNN) neural networks have been also investigated, in effort to exploit topological information within the power grid. Although promising results have been obtained, there lacks a systematic comparison between these architectures throughout literature. Accordingly, we assess the performance of a variety of FCNN, CNN and GNN models for two fundamental approaches to machine learning assisted OPF: regression (predicting optimal generator set-points) and classification (predicting the active set of constraints). For several synthetic grids with interconnected utilities, we show that locality properties between feature and target variables are scarce, hence find limited merit of harnessing topological information in NN models for this set of problems.

Index Terms—OPF, Graph Theory, Neural Networks

I. INTRODUCTION

OPTIMAL power flow (OPF) is an umbrella term for a family of constrained optimisation problems that govern electricity market dynamics and facilitate effective planning and operation of modern power systems [1, p. 514]. Classical (AC-)OPF formulates a non-linear and non-convex economic dispatch model, which minimises the cost of generator scheduling subject to reliability and security constraints of the grid. By virtue of competitive efficiency, optimal schedules are typically found using interior-point methods [2]. However, the required computation of the Hessian (second-order derivatives) of the Lagrangian at each optimisation step renders a super-linear time complexity, and so large-scale systems can be prohibitively slow to solve.

This computational constraint gives rise to several challenges for independent system operators (ISOs): (1) variable inclusion of certain generators (i.e. unit commitment) invokes binary variables in the optimisation model, thereby forming a mixed-integer, non-linear program (known to be NP-hard), exacerbating computational costs [3]; (2) the standard requirement for operators to satisfy $N-1$ security constraints (i.e. account for all contingency events where a single grid component fails) renders a much larger-scale problem, increasing the time complexity even further [4]; and lastly (3) modelling uncertainty in the supply-demand equilibrium induced by stochastic renewable generation requires methods such as scenario-based Monte-Carlo simulation [5], which necessitates sequential OPF solutions at rates unattainable by conventional algorithms.

To overcome these challenges, ISOs often resort to simplified OPF models by utilising convex relaxations [6] or linearizations [7], [8] such as the widely adopted DC-OPF model [9]. With considerably less control variables and constraints, DC-OPF can be solved very efficiently using interior-point or simplex methods [10, p. 224]. However, as DC-OPF solutions are in fact never feasible with respect to the full problem [11], set-points need to be found iteratively by manually updating the solution until convergence [12, p. 14] – hence DC-OPF is predisposed to sub-optimal generator scheduling.

In practice, ISOs typically leverage additional information about the grid in attempt to obtain solutions more efficiently. For instance, given the (reasonable) assumption that comparable grid states will correspond to neighbouring points in solution space, one can use the known solution to a similar problem as the starting value for the optimisation variables of another problem – a so-called *warm-start* (Figure 1, centre panel) –, rendering considerably faster convergence compared to arbitrary initialisation [13]. Alternatively, ISOs can capitalise on the observation that only a fraction of inequality constraints are actually binding at the optimal point [14], hence one can remove a large number of constraints from the mathematical model and formulate an equivalent, but significantly cheaper, *reduced problem* [15] (Figure 1, right panel). Security risks associated with the omission of violated constraints from the reduced problem can be mitigated by iteratively solving the reduced OPF and re-instating violated constraints until all constraints of the full problem are satisfied [16].

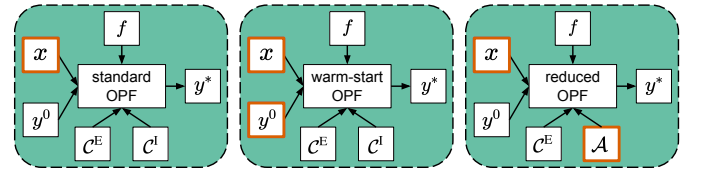


Fig. 1. Strategies for solving OPF with interior-point methods: standard (left), warm-start (centre) and reduced (right) problems. x and y are the vectors of grid parameters and optimisation variables, respectively, f is the objective function, C^E and C^I denote the sets of equality and inequality constraints, and $\mathcal{A} \subseteq C^I$ is the active subset of the inequality constraints. Typical varying arguments are highlighted in orange, whilst remaining arguments are potentially fixed.

A. Machine Learning Assisted OPF

A compelling new area of research borne from the machine learning community attempts to alleviate reliance on subpar OPF frameworks by fitting an estimator function on historical data. The estimators are typically neural networks (NNs) owed to their demonstrated ability to model complex non-linear

relationships with negligible online computation [17]. This makes it possible to obtain predictions in real-time, thereby shifting the computational expense from online optimisation to offline training – and the trained model can remain sufficient for a period of time, requiring only occasional re-training.

Most of the methods for machine learning assisted OPF can be generalised as one of two approaches: (1) *end-to-end* (or direct) models, where an estimator function is used to learn a direct mapping between the grid parameters and the optimal OPF solution; and (2) *hybrid* (or indirect) techniques – a two-step approach whereby an estimator function first maps the grid parameters to some quantities, which are subsequently used as inputs to an optimisation problem to find a (possibly exact) solution. Based on the actual target type, these methods can be further categorised depending on the type of predicted quantity: regression or classification.

1) *Regression*: By inferring OPF solutions directly, end-to-end regression methods bypass conventional solvers altogether, offering the greatest (online) computational gains [18]. However, since OPF is a constrained optimisation problem, the optimal solution is not necessarily a smooth function of the inputs: changes of the binding status of constraints can lead to abrupt changes of the optimal solution. Since the number of unique sets of binding constraints (i.e. congestion regimes) increases exponentially with system size, this approach requires training on relatively large data sets in order to obtain sufficient accuracy [19]. Moreover, there is no guarantee that the inferred optimal solution is feasible, and violation of important constraints poses severe security risks to the grid.

Instead, one can adopt a hybrid approach whereby the inferred optimal solution of the end-to-end method is used to initialise an interior-point solver (i.e. a warm-start), which provides an optimal solution to an optimisation problem equivalent to the original one (Figure 2). Compared to default heuristics used in the conventional optimisation method, an accurate initial point could theoretically reduce the number of required iterations (and so the computational cost) to reach the optimal point [20]. However, as discussed in [21], there are several practical issues which could arise, leading to limited computational gain for this technique.

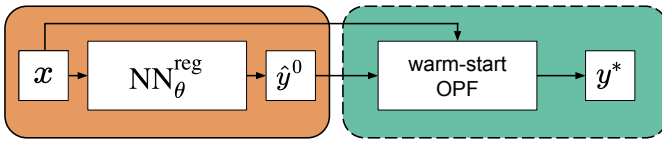


Fig. 2. Flowchart of the warm-start method (green panel) combined with a NN regressor (orange panel). For clarity, default arguments of the OPF operator are omitted.

2) *Classification*: An alternative hybrid approach leverages the aforementioned technique of formulating a reduced problem by removing non-binding inequality constraints from the mathematical model. A NN classifier is first used to predict the active set of constraints by either (1) identifying all distinct active sets in the training data and using a multi-class classifier to map the features accordingly [22]; or (2) by predicting the binding status of each inequality constraint using a binary multi-label classifier [21]. Since the number of active sets increases

exponentially with system size [23], the latter approach may be computationally favourable for larger grids.

To alleviate the security risks associated with imperfect classification, an *iterative feasibility test* can be employed to reinstate violated constraints until convergence, as detailed in [21] (Figure 3). Since the reduced OPF is much cheaper relative to the full problem, this can in theory be rather efficient.

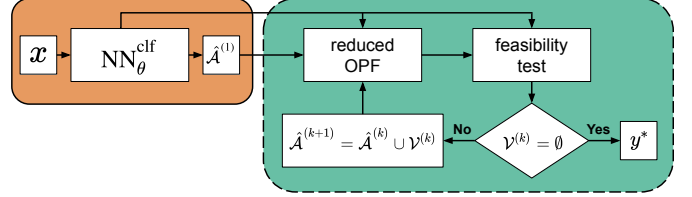


Fig. 3. Flowchart of the iterative feasibility test method (green panel) combined with a NN classifier (orange panel). $\hat{\mathcal{A}}^{(k)}$ and $\mathcal{V}^{(k)}$ are the sets of predicted active and violated inequality constraints at the k th step of the iterative feasibility test. For clarity, default arguments of OPF operator are omitted.

B. Contributions

Both the end-to-end and hybrid techniques for machine learning assisted OPF benefit from NN architectures designed to maximise predictive performance. Related works typically employ a range of shallow to deep fully-connected neural networks (FCNN). However, convolutional (CNN) [24] and graph (GNN) [25], [26], [27] neural networks have recently been investigated to exploit assumed locality properties within the power grid, i.e. whether the topology of the electricity network influences the correlation between inputs and outputs.

Building on this set of works, our contributions are as follows: (1) we introduce a concise framework for generalising end-to-end and hybrid methods for machine learning assisted OPF by characterising them as estimators of the corresponding OPF operator or function; (2) we provide a systematic comparison between the aforementioned NN architectures for both the regression and classification approaches, demonstrating the marginal utility of applying CNN and GNN architectures, hence recommended the application of FCNN models for such problems; (3) we show that locality properties between corresponding grid parameters (features or inputs) and generator set-points (targets or outputs) – essential for efficient inductive bias in both CNN and GNN models – are weak, which explains the moderate performance of these models compared to FCNN; and (4) we also show that a similar weak locality applies between grid parameters and locational marginal prices (LMPs), indicating that the applicability of CNN and GNN architectures would face similar challenges (and FCNN models may be preferred) if instead were used to predict these derived market signals.

II. METHODOLOGY

A. Problem Formulation

This work centres on the fundamental form of OPF, without consideration for unit commitment or security constraints (although machine learning assisted OPF can be readily extended to such cases [28], [29]). In general, OPF problems can be

expressed using the following concise form of mathematical programming:

$$\begin{aligned} \min_y \quad & f(x, y) \\ \text{s. t.} \quad & c_i^E(x, y) = 0 \quad i = 1, \dots, n \\ & c_j^I(x, y) \geq 0 \quad j = 1, \dots, m \end{aligned} \quad (1)$$

where x and y are the vectors of grid parameters and optimisation variables, respectively, $f(x, y)$ is the objective (or cost) function (parameterised by x), which is minimised with respect to y and subject to equality constraints $c_i^E(x, y) \in \mathcal{C}^E$ and inequality constraints $c_j^I(x, y) \in \mathcal{C}^I$. For convenience, we introduce \mathcal{C}^E and \mathcal{C}^I , which denote the sets of equality and inequality constraints with corresponding cardinalities $n = |\mathcal{C}^E|$ and $m = |\mathcal{C}^I|$. For instance, in a simple economic dispatch problem (the focus of this work), x includes the active and reactive power components of loads, y is a vector of voltage magnitudes and active powers of generators and the objective function is a quadratic or piece-wise linear function of the (monotonically increasing) generator cost curves. Equality constraints include the power balance and power flow equations, whilst inequality constraints impose lower and upper bounds on certain quantities.

B. OPF Operators and Functions

By formulating the problem in such a manner as eq. (1), one can view OPF as an operator, which maps the grid parameters (x) to the optimal value of the optimisation variables (y^*) [30]. In order to introduce a consistent framework, we extend the operator arguments by the objective (f) and constraint functions (\mathcal{C}^E and \mathcal{C}^I), as well as by the starting value of the optimisation variables (y^0). The value of y^0 has a considerable influence of the convergence rate of interior-point methods, and for non-convex formulations with multiple possible local minima, even the found optimum is a function of y^0 . The general form of the OPF operator can be written as¹:

$$\Phi : \Omega \rightarrow \mathbb{R}^{n_y} : \quad \Phi(x, y^0, f, \mathcal{C}^E, \mathcal{C}^I) = y^*, \quad (2)$$

where Ω is an abstract set within which the values of the operator arguments are allowed to change and n_y denotes the dimension of the optimisation variables. In the simplest case, only the grid parameters vary, whilst most arguments of the OPF operator remain fixed. Accordingly, we introduce a simpler notation, the OPF function, for such cases:

$$F_\Phi : \mathbb{R}^{n_x} \rightarrow \mathbb{R}^{n_y} : \quad F_\Phi(x) = y^*, \quad (3)$$

where n_x and n_y are the dimensions of the grid parameters and optimisation variables, respectively, whilst \mathcal{F}_Φ is used to denote the set of all feasible points, such that $y^* \in \mathcal{F}_\Phi$. Depending on the grid parameters, the problem may be infeasible: $\mathcal{F}_\Phi = \emptyset$.

¹We note that an even more general form of the operator can be defined when the arguments are mapped to the joint space of the primal and dual variables of the optimisation problem: $\Psi : \Omega \rightarrow \mathbb{R}^{n_y + n_z} : \quad \Psi(x, y^0, f, \mathcal{C}^E, \mathcal{C}^I) = (y^*, z^*)$, where z^* is the optimal value of the Lagrangian multipliers of the equality and inequality constraints. As locational marginal prices are computed from z^* , this formalism is useful to construct estimators for learning electricity prices.

C. Estimators of OPF Operators and Functions

Machine learning assisted OPF methods apply either an estimator operator or function, which both provide a computationally cheap prediction to the optimal point of the OPF based on the grid parameters, i.e. $\hat{\Phi}(x) = \hat{y}^* : \|\hat{y}^* - y^*\| < \varepsilon \wedge \mathbb{T}[\hat{\Phi}] \ll \mathbb{T}[\Phi]$ and $\hat{F}_\Phi(x) = \hat{y}^* : \|\hat{y}^* - y^*\| < \varepsilon \wedge \mathbb{T}[\hat{F}_\Phi] \ll \mathbb{T}[F_\Phi]$, where $\|\cdot\|$ is an arbitrary norm, ε is a threshold variable and \mathbb{T} denotes the computational time to obtain the solution.

1) *End-to-end*: To learn the optimal OPF solution directly from the grid parameters, NNs as regressors can be used, depicted by the following function:

$$\hat{F}_\Phi(x) = \text{NN}_\theta^{\text{reg}}(x) = \hat{y}^*, \quad (4)$$

where subscript θ denotes the NN parameters and the superscript *reg* indicates that the NN is used as a regressor. The problem dimensionality can be reduced by predicting only a subset of the optimisation variables – in this case, the remaining state variables can be easily obtained by solving the corresponding power flow problem [31], given the prediction is a feasible point. Optimal NN parameters can be obtained by minimising some loss function between the ground-truth y^* and prediction \hat{y}^* of some training set. Typically, the squared L2-norm, i.e. mean-squared error (MSE), is used: $\ell(y^*, \hat{y}^*) = \|y^* - \hat{y}^*\|_2^2$. To mitigate violations of certain constraints, a penalty term can be also added to this loss function [19].

2) *Warm-start*: Warm-start approaches utilise a hybrid model whereby a NN is first parameterised to infer an approximate set-point, $\hat{y}^0 = \text{NN}_\theta^{\text{reg}}(x)$, which is subsequently used to initialise the constrained optimisation procedure resulting in the exact solution (y^*):

$$\hat{\Phi}^{\text{warm}}(x) = \Phi(x, \hat{y}^0, f, \mathcal{C}^E, \mathcal{C}^I) \quad (5)$$

$$= \Phi(x, \text{NN}_\theta^{\text{reg}}(x), f, \mathcal{C}^E, \mathcal{C}^I) \quad (6)$$

$$= y^*. \quad (7)$$

Optimal NN parameters can be obtained by minimising a similar conventional loss function as in the case of the end-to-end approach. However, significant improvement has been demonstrated by optimising NN parameters with respect to a (meta-)loss function corresponding directly to the time complexity of the entire pipeline (i.e. including the warm-started OPF) [32]: $\ell(\hat{y}^0) = \mathbb{T}[\Phi(x, \hat{y}^0, f, \mathcal{C}^E, \mathcal{C}^I)]$.

3) *Reduced problem*: In this hybrid approach, a binary multi-label NN classifier ($\text{NN}_\theta^{\text{clf}}$) is used to predict the active set of constraints, and a reduced OPF problem is formulated, which maintains the same objective function as the original full problem:

$$\hat{\Phi}^{\text{red}}(x) = \Phi(x, y^0, f, \mathcal{C}^E, \hat{\mathcal{A}}) \quad (8)$$

$$= \Phi(x, y^0, f, \mathcal{C}^E, \text{NN}_\theta^{\text{clf}}(x)) \quad (9)$$

$$= \hat{y}^*, \quad (10)$$

where $\mathcal{A} \subseteq \mathcal{C}^I$ is the active subset of the inequality constraints and $\hat{\mathcal{A}}$ is the predicted active set. It should also be noted that

$\mathcal{C}^E \cup \mathcal{A}$ contains all active constraints defining the specific congestion regime. In the case of a multi-label classifier, the output is a binary vector representing an enumeration of the set of non-trivial constraints, learnt by minimising the binary cross-entropy loss (BCE) between the ground-truths represented by \mathcal{A} and the predicted binding probabilities of constraints defining $\hat{\mathcal{A}}$: $\ell(\mathcal{A}, \hat{\mathcal{A}}) = -\sum_j c_j \log \hat{c}_j + (1 - c_j) \log(1 - \hat{c}_j)$.

Violated constraints omitted from the reduced model are retained using the aforementioned iterative feasibility test to ensure convergence to an optimal point of the full problem. The computational gain can again be further enhanced via meta-optimisation by directly encoding the time complexity into a (meta-)loss function and optimising the NN weights accordingly [21]: $\ell(\hat{\mathcal{A}}) = \mathbb{T} \left[\Phi \left(x, y^0, f, \mathcal{C}^E, \hat{\mathcal{A}} \right) \right]$.

D. Architectures

Power grids are complex networks consisting of buses (e.g. generation points, load points etc.) connected by transmission lines, hence can conveniently be depicted as an un-directed graph $\mathbb{G} = (\mathcal{N}, \mathcal{E})$, where \mathcal{N} and $\mathcal{E} \subseteq \mathcal{N} \times \mathcal{N}$ denote the sets of nodes and edges (Figure 4). Also, \mathcal{G} and \mathcal{L} will denote the sets of generators and loads, respectively.

This formulation motivates the use of NN architectures specifically designed to leverage the spatial dependencies within non-Euclidean data structures, i.e. GNN models – the hypothesis being that OPF problems exhibit a locality property whereby the network topology influences to correlation between grid parameters and the subsequent solution.

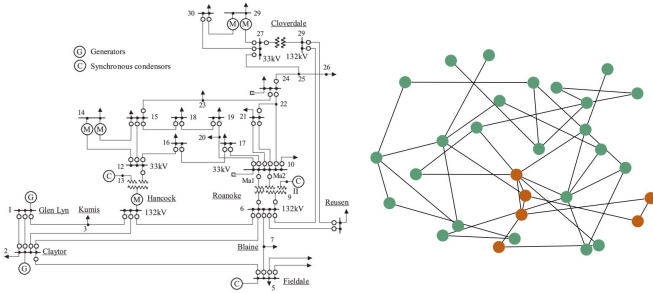


Fig. 4. Schematic diagram [33] (left) and corresponding graphical representation (right) for synthetic grid case30-ieee. Orange and green circles denote generator and load buses, respectively.

In real power grids, however, a given bus can include multiple generators and loads, which, although can have different power supply and demand, share the bus voltage. To accommodate such characteristics in GNN models straightforwardly, we use a transformed version of the original graph ($\mathbb{G}' = (\mathcal{N}', \mathcal{E}')$), where each node of the transformed network represents either a single generator or a load (i.e. $|\mathcal{N}'| = |\mathcal{G}| + |\mathcal{L}|$), and generators and loads belonging to the same bus of the original network are interconnected. With this representation of the grid, generator real power outputs are obtained as individual nodal features, while bus voltage magnitudes are computed as averages of the corresponding individual voltages.

1) *FCNN*: Fully connected NN models, denoted by $\mathcal{M}^{\text{FCNN}}$, are used here as baseline. Their input domain is equivalent to the raw vector of grid parameters, i.e. active and reactive power components of loads: $x \in \mathbb{R}^{2|\mathcal{L}|}$, while the corresponding output vector includes the generators' injected active power and the voltage magnitude at buses comprising at least one generator ($\mathcal{N}^{\text{gen}} \in \mathcal{N}$), i.e. $y \in \mathbb{R}^{|\mathcal{G}| + |\mathcal{N}^{\text{gen}}|}$. Since FCNN is defined in an un-structured data space, this baseline theoretically lacks sufficient relational inductive bias to efficiently exploit any underlying spatial dependencies – this information could be learnt implicitly through optimisation, but possibly requires a highly flexible model with a large amount of data, scaling poorly to large-scale OPF problems [34]. We investigated two FCNN models using one ($\mathcal{M}_{\text{global-1}}^{\text{FCNN}}$) and three ($\mathcal{M}_{\text{global-3}}^{\text{FCNN}}$) hidden layers.

2) *CNN*: We explore the utility of augmenting the fully-connected layers with an antecedent sequence of convolutional and pooling layers ($\mathcal{M}_{\text{global-4}}^{\text{CNN}}$), designed to extract a spatial hierarchy of latent features, which are subsequently (non-linearly) mapped to the target. A reasonable assumption here is that one can leverage spatial correlations within pseudo-images of the electrical grid using the (weighted) adjacency matrix. However, convolutions in Euclidean space are dependent upon particular geometric priors, which are not observed in the graph domain (e.g. shift-invariance), hence filters can no longer be node-agnostic, and the lack of natural order means operations need to instead be permutation invariant. Nevertheless, we validate this conjecture using CNNs by combining each load constituent of length $|\mathcal{N}'|$ into a 3-dimensional tensor, i.e. $x \in \mathbb{R}^{2 \times |\mathcal{N}'| \times |\mathcal{N}'|}$.

3) *GNN*: We analyse several GNN architectures whereby the binary adjacency matrix is used to extract latent features by propagating information across neighbouring nodes irrespective of the input sequence [35]. Such propagation is achieved using graph convolutions, which can be broadly categorised as either spectral or spatial filtering [36].

Spectral filtering adopts methods from graph signal processing: operations occur in the Fourier domain whereby input signals are passed through parameterised functions of the normalised graph Laplacian, thereby exploiting its positive-semidefinite property. Given this procedure has $\mathcal{O}(|\mathcal{N}'|^3)$ time complexity, we investigate four spectral layers designed to reduce computational costs by avoiding full eigendecomposition of the Laplacian: (1) *ChebConv* (\mathcal{M}^{CHC}), which uses approximate filters derived from Chebyshev polynomials of the eigenvalues up to the K -th order [37]; (2) *GCNConv* (\mathcal{M}^{GCN}), which constrains the layer-wise convolution to first-order neighbours ($K = 1$), lessening overfitting to particular localities [38]; (3) *GraphConv* (\mathcal{M}^{GC}), which is analogous to *GCNConv* except adopts a discrete weight matrix for self-connections [39]; and (4) *GATConv* (\mathcal{M}^{GAT}), which extends the message passing framework of *GCNConv* by assigning each edge with relative importance through attention coefficients [40]. Note that all GNN models are named in accordance with the PyTorch Geometric library [41].

By contrast, spatial graph convolutions (a non-Euclidean generalisation of the convolution operation found in CNNs) are performed directly in the graph domain, reducing the

computational complexity whilst minimising loss of structural information – a byproduct of reducing to embedded space [42]. We investigate *SplineConv* (\mathcal{M}^{SC}) [43] which, for a given node, computes a linear combination of its features together with those of its K -th order neighbours, weighted by a kernel function – the product of parameterised B-spline basis functions. The local support property of B-splines reduces the number of parameters, enhancing the computational efficiency of the operator.

E. Technical Details

1) *Samples*: To span multiple grid sizes, we built test cases using several synthetic grids from the Power Grid Library [44] ranging from 24 – 2853 buses. To maintain validity of the constructed data sets whilst ensuring a thorough exploration of congestion regimes, we generated 10k (feasible) samples for each synthetic grid by re-scaling each active and reactive load component (relative to nominal values) by factors independently drawn from a uniform distribution, $\mathcal{U}(0.8, 1.2)$. OPF solutions were obtained using *PowerModels.jl* [45] (an OPF package written in Julia [46]) in combination with the IPOPT solver [2].

2) *Neural Networks*: Our model with the largest number of parameters was a three hidden layer fully-connected model ($\mathcal{M}_{\text{global-3}}^{\text{FCNN}}$) that also served as the baseline. The size of each hidden layer was computed through a linear interpolation between the corresponding input and output sizes.

In the case of CNN, each model was constructed using 3×1 kernels, 1-dimensional max-pooling layers, zero-padding and a stride length of 1.

For GNN models, we investigated three architecture types: (1) the first type included two convolutional layers followed by a fully-connected readout layer making the original local structure non-local ($\mathcal{M}_{\text{global-3}}^{\text{GNN}}$); (2) in the second type, only three convolutional layers were present, simply treating the features available locally at each node as the output ($\mathcal{M}_{\text{local-3}}^{\text{GNN}}$); and lastly (3) the third type was again a global one extending the above local type with a fully-connected readout layer ($\mathcal{M}_{\text{global-4}}^{\text{GNN}}$). While corresponding $\mathcal{M}_{\text{global-3}}^{\text{GNN}}$ and $\mathcal{M}_{\text{local-3}}^{\text{GNN}}$ models were constructed to have an approximately equal number of parameters (details discussed below), $\mathcal{M}_{\text{global-4}}^{\text{GNN}}$ models had a significantly larger number of parameters due to the additional readout layer. For \mathcal{M}^{CHC} and \mathcal{M}^{SC} models, hyperparameter K was set to 4.

Since our aim was to compare the predictive performance of models with and without topology based inductive bias, the single layer FCNN, CNN and several GNN architectures were constructed to have a similar number of parameters for each synthetic grid. This required scaling the number of channels of the hidden layers of some architectures according to the grid size (σ_s) and the model type (σ_m). The actual number of channels used for the CNN and GNN models is presented in Table I.

For each grid, the generated 10k samples were split into training, validation and test sets with a ratio of 80:10:10. In all cases, the ADAM [47] optimizer was applied (with default parameters $\beta_1 = 0.9$ and $\beta_2 = 0.999$ and learning-rate $\eta = 10^{-4}$)

TABLE I
NUMBER OF CHANNELS USED FOR CNN AND GNN ARCHITECTURES. σ_s AND σ_m ARE THE GRID SIZE AND MODEL TYPE BASED SCALING FACTORS. n_n DENOTES THE NUMBER OF NODES OF THE TRANSFORMED NETWORK AND n_y IS THE NUMBER OF OUTPUT VARIABLES.

$$\sigma_s = \begin{cases} 1 & \text{if } |\mathcal{N}| \leq 72 \\ 2 & \text{if } |\mathcal{N}| > 72 \end{cases} \quad \sigma_m = \begin{cases} 1 & \text{if } \mathcal{M} = \mathcal{M}^{\text{GCN}} \text{ or } \mathcal{M}^{\text{GAT}} \\ 0.5 & \text{if } \mathcal{M} = \mathcal{M}^{\text{CHC}} \end{cases}$$

GNN layer	$\mathcal{M}_{\text{global-4}}^{\text{CNN}}$	$\mathcal{M}_{\text{global-3}}^{\text{GNN}}$	$\mathcal{M}_{\text{local-3}}^{\text{GNN}}$	$\mathcal{M}_{\text{global-4}}^{\text{GNN}}$
1.	4	$8\sigma_s$	8	8
2.	8	$16\sigma_s$	$n_n\sigma_m$	$n_n\sigma_m$
3.	16	—	$n_y\sigma_s\sigma_m$	$n_y\sigma_s\sigma_m$
Readout layer	yes	yes	no	yes

using an early stopping with a patience of 20 determined on the validation set. Mini-batch size of 100 was applied and hidden layers were equipped with BatchNorm [48] and a ReLU [49] activation function was used. For each model, statistics (mean and 95% confidence interval) of the predictive performance were computed using 10 independent runs.

Models were implemented in Python 3.0 using PyTorch [50] and PyTorch Geometric [41] libraries. Experiments were carried out on NVIDIA Tesla M60 GPUs. In order to facilitate research reproducibility in the field, we have made the generated samples, as well as our code, publicly available at <https://github.com/tdfalc/ml-opf>.

III. NUMERICAL RESULTS

A. Regression

We begin our analysis with the predictive performance of the architectures that encode the targets as global variables. Table II shows the MSE statistics of the investigated models for each grid. The first column includes the results of our baseline $\mathcal{M}_{\text{global-3}}^{\text{FCNN}}$ model, which has the largest number of parameters (Table III). In the presence of appropriate locality attributes, CNN and GNN models are expected to provide a comparable performance to $\mathcal{M}_{\text{global-3}}^{\text{FCNN}}$ with a significantly smaller amount of parameters due to their topology based inductive bias.

In order to investigate the predictive performance with and without topological information, we first constructed global FCNN ($\mathcal{M}_{\text{global-1}}^{\text{FCNN}}$), CNN ($\mathcal{M}_{\text{global-4}}^{\text{CNN}}$) and GNN ($\mathcal{M}_{\text{global-3}}^{\text{GNN}}$) models in a manner such that they have a similar number of parameters for each grid (Table III).

In general, the regression performance of the investigated models (including the baseline) has a weak correlation with the system size. This indicates that other factors, for instance the actual number of active sets, can also play an important role (as observed previously in [21]).

Comparing the CNN and GNN models, we found that in most of the cases, GNN models outperform the CNN model. An interesting exception is case57-ieee, where the CNN model appeared to perform best. However, we rather consider this as an anomalous case, where the reduced error could be attributed to the coincidental unearthing of structural information within the receptive fields when convolving over the pseudo-image of the grid.

TABLE II
MSE STATISTICS (MEAN AND 95% CONFIDENCE INTERVALS) OF THE TEST SETS FOR GLOBAL REGRESSION MODELS

Case	MSE ($\times 10^{-3}$)							
	$\mathcal{M}_{\text{global-3}}^{\text{FCNN}}$	$\mathcal{M}_{\text{global-1}}^{\text{FCNN}}$	$\mathcal{M}_{\text{global-4}}^{\text{CNN}}$	$\mathcal{M}_{\text{global-3}}^{\text{GCN}}$	$\mathcal{M}_{\text{global-3}}^{\text{CHC}}$	$\mathcal{M}_{\text{global-3}}^{\text{SC}}$	$\mathcal{M}_{\text{global-3}}^{\text{GC}}$	$\mathcal{M}_{\text{global-3}}^{\text{GAT}}$
case24-ieee-rtts	0.18 \pm 0.02	0.94 \pm 0.04	1.55 \pm 0.21	2.65 \pm 0.13	0.70 \pm 0.04	1.10 \pm 0.12	1.04 \pm 0.06	2.76 \pm 0.19
case30-ieee	0.05 \pm 0.01	0.03 \pm 0.01	0.62 \pm 0.22	3.25 \pm 0.82	0.09 \pm 0.01	0.27 \pm 0.08	0.26 \pm 0.12	3.06 \pm 0.33
case39-epri	0.89 \pm 0.10	3.16 \pm 0.09	7.01 \pm 0.09	4.30 \pm 0.23	2.38 \pm 0.10	3.00 \pm 0.09	2.74 \pm 0.13	4.72 \pm 0.35
case57-ieee	0.52 \pm 0.11	1.62 \pm 0.15	1.22 \pm 0.10	2.18 \pm 0.13	1.28 \pm 0.14	1.64 \pm 0.14	1.59 \pm 0.14	2.28 \pm 0.13
case73-ieee-rtts	0.21 \pm 0.07	0.69 \pm 0.02	1.06 \pm 0.13	1.59 \pm 0.11	0.65 \pm 0.05	0.85 \pm 0.11	0.85 \pm 0.07	1.85 \pm 0.21
case118-ieee	0.39 \pm 0.03	1.28 \pm 0.07	3.68 \pm 0.75	2.39 \pm 0.12	1.23 \pm 0.07	1.24 \pm 0.07	1.27 \pm 0.13	2.50 \pm 0.10
case162-ieee-dtc	2.61 \pm 0.10	3.19 \pm 0.08	3.28 \pm 0.15	4.77 \pm 0.21	3.08 \pm 0.10	2.90 \pm 0.11	3.04 \pm 0.10	4.87 \pm 0.23
case300-ieee	2.06 \pm 0.06	2.86 \pm 0.05	3.95 \pm 0.22	3.24 \pm 0.09	2.42 \pm 0.04	2.47 \pm 0.20	2.39 \pm 0.06	3.56 \pm 0.19
case588-sdet	2.56 \pm 0.06	3.12 \pm 0.05	4.10 \pm 0.20	4.62 \pm 0.36	3.25 \pm 0.07	3.00 \pm 0.06	3.05 \pm 0.05	5.07 \pm 0.30
case1354-pegase	0.83 \pm 0.12	1.30 \pm 0.09	2.78 \pm 0.23	2.16 \pm 0.17	1.43 \pm 0.09	1.35 \pm 0.10	1.35 \pm 0.12	2.51 \pm 0.15
case2853-sdet	5.99 \pm 0.16	6.87 \pm 0.05	15.71 \pm 0.93	10.15 \pm 0.58	9.70 \pm 0.33	8.64 \pm 0.29	8.49 \pm 0.41	11.01 \pm 0.46

TABLE III
NUMBER OF PARAMETERS FOR GLOBAL REGRESSION MODELS

Case	# of parameters							
	$\mathcal{M}_{\text{global-3}}^{\text{FCNN}}$	$\mathcal{M}_{\text{global-1}}^{\text{FCNN}}$	$\mathcal{M}_{\text{global-4}}^{\text{CNN}}$	$\mathcal{M}_{\text{global-3}}^{\text{GCN}}$	$\mathcal{M}_{\text{global-3}}^{\text{CHC}}$	$\mathcal{M}_{\text{global-3}}^{\text{SC}}$	$\mathcal{M}_{\text{global-3}}^{\text{GC}}$	$\mathcal{M}_{\text{global-3}}^{\text{GAT}}$
case24-ieee-rtts	6575	2156	1336	2303	2783	2943	2463	2353
case30-ieee	4436	732	984	607	1087	1247	767	657
case39-epri	7877	1580	1568	1035	1515	1675	1195	1085
case57-ieee	13933	1610	1722	1047	1527	1687	1207	1097
case73-ieee-rtts	58677	19404	15504	18715	19195	19355	18875	18765
case118-ieee	91835	25596	23160	26354	28178	28786	26962	26454
case162-ieee-dtc	104396	7800	7524	8558	10382	10990	9166	8658
case300-ieee	440480	82938	78006	83696	85520	86128	84304	83796
case588-sdet	1512583	207152	200700	212838	214662	215270	213446	212938
case1354-pegase	8486627	1408680	1390548	1409438	1411262	1411870	1410046	1409538
case2853-sdet	42568525	9233926	9166558	9299404	9301228	9301836	9300012	9299504

Although GCN is the simplest GNN model we investigated, in general it performs similarly to the more sophisticated GAT model. Whilst CHC and SC models have similar performance, computational efficiencies with respect to the training times of CHC (Table IV) allude to a better scaling to larger grids.

The most striking observation is that the single-layer FCNN model exhibits exceedingly comparable performance to the best GNN models and for the two largest grids, it even outperforms all GNN models. It is also worth mentioning that $\mathcal{M}_{\text{global-1}}^{\text{FCNN}}$ has at least one order of magnitude shorter training times than the global GNN models (Table IV). For many cases, the significantly larger $\mathcal{M}_{\text{global-3}}^{\text{FCNN}}$ model had an even shorter training time than $\mathcal{M}_{\text{global-1}}^{\text{FCNN}}$ due to the faster convergence.

The moderate performance of the global GNN models could be a result of the readout layer simply inducing noise in the system by arbitrarily mixing signals of nodes further away in the system. To investigate this possibility, we performed a set of experiments up to grid size of 588, this time with local architectures for the GCN, CHC and GAT models (left three columns of Table V). Interestingly, although the number of parameters of these local models is comparable to that of the global models (Table VI), the observed performance of each of the three GNN models is considerably worse. This suggests that the main contribution to the predictive capacity actually stems from the readout layer and also indicates a potential lack of locality properties.

To further validate the above arguments, we investigated the effect of extending the local models with a readout layer, i.e. converting the local regression models to their global counterpart. We found that using the readout layer significantly improved the predictive performance for all cases (right three columns of Table V).

One could argue that the improvement is due to the increased number of parameters, which did indeed approximately double (Table VI). However, comparing the performance of two sets of global models, the difference seems to be marginal, highlighting again the utility of the fully-connected component and confirming our suspicion of a lack of locality within this problem.

B. Classification

In principle, the binding status of constraints could be predicted as nodal and edge features within a GNN framework. However, based on our findings for the regression experiments (i.e. that the global strategy significantly outperforms the local one), we treated constraints only as global variables. Classification performance is reported in terms of statistics of BCE of the test set, again based on 10 independent runs (Table VII). Additional tables concerning the number of parameters as well as the training time for each model can be found in the *Supplementary Materials*.

TABLE IV
TRAINING TIME STATISTICS (MEAN AND 95% CONFIDENCE INTERVALS) FOR GLOBAL REGRESSION MODELS

Case	Training time ($\times 10^2$ s)							
	$\mathcal{M}_{\text{global-3}}^{\text{FCNN}}$	$\mathcal{M}_{\text{global-1}}^{\text{FCNN}}$	$\mathcal{M}_{\text{global-4}}^{\text{CNN}}$	$\mathcal{M}_{\text{global-3}}^{\text{GCN}}$	$\mathcal{M}_{\text{global-3}}^{\text{CHC}}$	$\mathcal{M}_{\text{global-3}}^{\text{SC}}$	$\mathcal{M}_{\text{global-3}}^{\text{GC}}$	$\mathcal{M}_{\text{global-3}}^{\text{GAT}}$
case24-ieee-rtts	0.75 ± 0.14	3.40 ± 0.47	1.60 ± 0.31	12.06 ± 1.76	20.78 ± 1.97	10.80 ± 1.87	11.81 ± 1.67	15.56 ± 2.64
case30-ieee	0.57 ± 0.05	0.58 ± 0.04	1.07 ± 0.22	9.75 ± 3.03	16.04 ± 1.96	9.22 ± 1.30	14.06 ± 3.55	22.30 ± 6.16
case39-epri	0.58 ± 0.10	0.82 ± 0.05	0.83 ± 0.17	12.23 ± 1.70	16.36 ± 2.90	8.69 ± 1.17	9.70 ± 0.74	15.66 ± 3.34
case57-ieee	0.33 ± 0.08	0.67 ± 0.03	1.13 ± 0.17	12.73 ± 1.83	12.39 ± 2.99	9.20 ± 2.33	11.93 ± 2.10	13.69 ± 2.22
case73-ieee-rtts	0.83 ± 0.15	2.79 ± 0.12	1.64 ± 0.21	12.36 ± 1.82	19.13 ± 2.19	10.07 ± 1.49	12.29 ± 1.92	16.36 ± 2.53
case118-ieee	0.43 ± 0.09	1.98 ± 0.18	1.66 ± 0.28	17.80 ± 2.44	8.25 ± 0.96	7.10 ± 0.77	5.73 ± 0.53	20.62 ± 1.99
case162-ieee-dtc	0.28 ± 0.04	1.32 ± 0.17	1.08 ± 0.23	14.13 ± 2.56	6.45 ± 0.83	8.49 ± 1.69	7.44 ± 1.29	12.19 ± 1.89
case300-ieee	0.33 ± 0.02	0.64 ± 0.05	1.70 ± 0.27	14.74 ± 1.94	11.87 ± 1.01	13.25 ± 1.63	8.43 ± 1.23	16.91 ± 5.28
case588-sdet	0.65 ± 0.15	0.58 ± 0.05	1.84 ± 0.40	23.74 ± 6.36	11.24 ± 1.26	15.54 ± 3.02	10.72 ± 1.63	22.61 ± 4.16
case1354-pegase	1.81 ± 0.22	1.13 ± 0.11	1.52 ± 0.43	18.07 ± 3.34	22.55 ± 1.46	26.74 ± 5.08	13.74 ± 1.77	21.54 ± 2.84
case2853-sdet	9.54 ± 0.44	1.37 ± 0.05	0.54 ± 0.02	14.72 ± 1.00	16.93 ± 0.88	24.35 ± 2.19	14.38 ± 1.24	17.29 ± 3.29

TABLE V
MSE STATISTICS (MEAN AND 95% CONFIDENCE INTERVALS) OF THE TEST SETS FOR LOCAL AND EXTENDED GLOBAL REGRESSION GNN MODELS

Case	MSE ($\times 10^{-3}$)					
	$\mathcal{M}_{\text{local-3}}^{\text{GCN}}$	$\mathcal{M}_{\text{local-3}}^{\text{CHC}}$	$\mathcal{M}_{\text{local-3}}^{\text{GAT}}$	$\mathcal{M}_{\text{global-4}}^{\text{GCN}}$	$\mathcal{M}_{\text{global-4}}^{\text{CHC}}$	$\mathcal{M}_{\text{global-4}}^{\text{GAT}}$
case24-ieee-rtts	73.93 ± 8.46	27.03 ± 0.36	63.69 ± 9.76	2.63 ± 0.12	0.50 ± 0.04	2.48 ± 0.12
case30-ieee	29.83 ± 5.39	0.23 ± 0.05	19.45 ± 6.46	2.39 ± 0.12	0.06 ± 0.01	2.84 ± 0.13
case39-epri	14.46 ± 2.84	3.27 ± 0.18	15.09 ± 2.92	2.81 ± 0.14	2.11 ± 0.07	3.24 ± 0.19
case57-ieee	8.53 ± 3.65	2.29 ± 0.15	9.80 ± 4.50	2.14 ± 0.15	1.09 ± 0.17	2.35 ± 0.22
case73-ieee-rtts	36.85 ± 1.53	31.69 ± 0.11	53.01 ± 1.03	1.31 ± 0.14	0.35 ± 0.04	1.67 ± 0.13
case118-ieee	31.57 ± 3.29	6.47 ± 0.20	39.85 ± 7.85	3.91 ± 0.09	1.41 ± 0.09	4.34 ± 0.27
case162-ieee-dtc	11.71 ± 0.61	6.27 ± 0.18	11.81 ± 0.60	6.40 ± 0.12	3.47 ± 0.11	5.55 ± 0.14
case300-ieee	16.79 ± 2.59	9.35 ± 0.15	46.63 ± 8.50	3.48 ± 0.08	2.83 ± 0.08	5.01 ± 1.34
case588-sdet	19.98 ± 2.27	16.30 ± 0.24	22.48 ± 0.95	5.64 ± 0.18	4.20 ± 0.07	15.51 ± 2.25

TABLE VI
NUMBER OF PARAMETERS FOR LOCAL AND EXTENDED GLOBAL REGRESSION GNN MODELS

Case	# of parameters					
	$\mathcal{M}_{\text{local-3}}^{\text{GCN}}$	$\mathcal{M}_{\text{local-3}}^{\text{CHC}}$	$\mathcal{M}_{\text{local-3}}^{\text{GAT}}$	$\mathcal{M}_{\text{global-4}}^{\text{GCN}}$	$\mathcal{M}_{\text{global-4}}^{\text{CHC}}$	$\mathcal{M}_{\text{global-4}}^{\text{GAT}}$
case24-ieee-rtts	2796	3165	2996	6888	7257	7088
case30-ieee	796	1045	900	1528	1777	1632
case39-epri	1355	1629	1493	2935	3209	3073
case57-ieee	1541	1935	1703	3151	3545	3313
case73-ieee-rtts	20583	21451	21145	57411	58279	57973
case118-ieee	27912	28835	28600	53508	54431	54196
case162-ieee-dtc	9844	10969	10284	17644	18769	18084
case300-ieee	87526	89662	88698	170464	172600	171636
case588-sdet	220332	224469	222260	432412	436549	434340

Here, the single-layer FCNN was observed to be even more dominant relative to the regression case. Interestingly, for larger grids it even outperforms the three-layer FCNN, which could be suffering from over-fitting as a consequence of increased flexibility. In general, we reach a similar conclusion as in the global regression setting, whereby the performance enhancements of the GNN classifiers are marginal respective to their practicality and computational limitations. CHC and SC models perform similarly, but CHC remains the cheaper option with respect to the training time. Note that GAT was excluded from these experiments since it had already shown weak performance for the regression case relative to the other GNN models.

Although for brevity we only present the test set loss, we also note that we observed a greater precision than recall in virtually every instance. This implies that the BCE objective is more sensitive to false positives. In combination with the iterative feasibility test, which is more sensitive to false negative predictions, this can result in a significant increase in the computational cost of obtaining solutions [21]. In order to fix this misalignment, one could either use a weighted BCE (with appropriate weights for the corresponding terms) or a meta-loss objective function [32] [21].

TABLE VII
BCE STATISTICS (MEAN AND 95% CONFIDENCE INTERVALS) OF THE TEST SETS FOR GLOBAL CLASSIFICATION MODELS

Case	BCE ($\times 10^{-2}$)						
	$\mathcal{M}_{\text{global-3}}^{\text{FCNN}}$	$\mathcal{M}_{\text{global-1}}^{\text{FCNN}}$	$\mathcal{M}_{\text{global-4}}^{\text{CNN}}$	$\mathcal{M}_{\text{global-3}}^{\text{GNN}}$	$\mathcal{M}_{\text{global-3}}^{\text{CHC}}$	$\mathcal{M}_{\text{global-3}}^{\text{SC}}$	$\mathcal{M}_{\text{global-3}}^{\text{GC}}$
case24-ieee-rtts	1.89 ± 0.10	3.58 ± 0.12	4.66 ± 0.52	6.93 ± 0.65	3.14 ± 0.18	3.52 ± 0.21	3.42 ± 0.33
case30-ieee	1.71 ± 0.31	5.14 ± 0.65	4.00 ± 0.55	8.76 ± 1.24	3.58 ± 0.28	5.33 ± 1.21	4.98 ± 0.73
case39-epri	3.61 ± 0.12	7.55 ± 0.21	13.84 ± 0.22	10.48 ± 0.31	7.07 ± 0.15	8.07 ± 0.26	7.60 ± 0.35
case57-ieee	1.67 ± 0.14	2.51 ± 0.24	2.51 ± 0.29	2.81 ± 0.17	2.34 ± 0.18	2.24 ± 0.24	2.12 ± 0.18
case73-ieee-rtts	3.06 ± 0.14	4.34 ± 0.10	4.71 ± 0.25	6.28 ± 0.24	3.34 ± 0.11	4.26 ± 0.59	4.08 ± 0.89
case118-ieee	4.51 ± 0.25	6.19 ± 0.21	8.29 ± 0.39	7.86 ± 0.32	4.65 ± 0.19	4.35 ± 0.21	4.40 ± 0.20
case162-ieee-dtc	5.42 ± 0.29	6.27 ± 0.15	6.31 ± 0.34	8.32 ± 0.19	6.19 ± 0.18	5.99 ± 0.17	6.18 ± 0.18
case300-ieee	9.32 ± 0.23	8.43 ± 0.14	10.97 ± 0.29	10.20 ± 0.33	8.86 ± 0.19	8.70 ± 0.16	8.65 ± 0.21
case588-sdet	10.92 ± 0.22	8.75 ± 0.14	12.13 ± 0.45	12.14 ± 0.37	11.38 ± 0.21	11.46 ± 0.18	10.92 ± 0.14
case1354-pegase	11.99 ± 0.18	10.56 ± 0.10	21.56 ± 0.98	17.14 ± 0.44	18.80 ± 0.32	18.43 ± 0.93	17.86 ± 0.60
case2853-sdet	17.30 ± 0.36	11.55 ± 0.04	37.88 ± 1.59	28.58 ± 0.88	31.83 ± 0.33	30.37 ± 0.53	33.47 ± 0.61

C. Locality Properties

Experimental results for the NN models indicated that the general assumption of locality may not be appropriate for this problem, i.e. there is only a weak – or no existence of – locality between load inputs and generator set-point outputs. To explore this relationship further, we carried out a sensitivity analysis that directly measures locality: for each synthetic grid, we iteratively perturbed each active load of 100 configurations by 1% and recorded the absolute value of the relative change in voltage magnitude and active power injection of each generator (i.e. $\left| \frac{dV_m^j}{dP_l^i} \right|$ and $\left| \frac{dP_g^j}{dP_l^i} \right|$, where P_l^i are the active loads with $i = 1, \dots, |\mathcal{L}|$; and V_m^j and P_g^j are the voltage magnitude and injected active power of generators with $j = 1, \dots, |\mathcal{G}|$), as a function of neighbourhood order (i.e. the topological distance from the perturbed load). If a grid were to exhibit locality properties, one would expect a distinct negative correlation between the average of these quantities and the respective distance from the perturbed load within the graph domain.

The results of the sensitivity analysis are shown in the left panels of Figure 5. Although there are certain cases where either the voltage magnitude or active power injection shows a weak anti-correlation with the topological distance, in general we found no evidence that the topology of the network influences the correlation between input and output variables. Plotting the distribution of generators as a function of distance from the perturbed load (middle panels of Figure 5) suggests that this result should be of no surprise: as the system size increases, so does the average distance between the perturbed load and the generators in the system, which decreases the likelihood that nearby generators will balance corresponding demand (for apparent physical reasons such as generator capacity, line congestion etc.).

Finally, we also explored the existence of possible locality within the LMPs, which are functions of the duals (shadow prices) [51]. If a stronger locality property were to exist here this would be promising for using GNN models to predict electricity prices [52]. However, as shown in the right panels of Figure 5, we found no evidence of locality for the LMP values either, alluding to limited performance here as well for GNN models compared to FCNN.

IV. CONCLUSION

With the potential to shift the entire computational effort to offline training, machine learning assisted OPF has become an interesting research direction. Neural network based approaches are particularly promising as they can effectively model complex non-linear relationships between grid parameters and primal or dual variables of the underlying OPF problem.

Although most related works have applied fully-connected neural networks so far, these networks scale relatively poorly with system size. Therefore, incorporating topological information of the electricity grid into the inductive bias of some graph neural network is a sensible step towards reducing the number of NN parameters.

In this paper, we first provided a general framework of the most widely used end-to-end and hybrid techniques and showed that they can be considered as estimators of the OPF operator or function.

We then presented a systematic comparison of several NN architectures including FCNN, CNN and GNN models. We found that in general, an FCNN model has a comparable or even better predictive performance than global CNN and GNN models with similar number of parameters. The moderate performance of the CNN model can be explained by the fact that it carries out convolutions in the Euclidean space (instead of the graph domain). We also identified that in the case of global GNN models, the readout layer plays a key role: constructing local models by removing their readout layer led to a significant decline in the predictive performance.

The results indicated that the required assumption of locality between grid parameters (inputs) and generator set-points (outputs) might not hold. To validate the findings of the NN experiments, by carrying out a sensitivity analysis we showed that locality properties are indeed scarce between grid parameters and primal variables of the OPF. Additionally, we found a similar lack of locality between grid parameters and LMPs. Therefore, we conclude that for predicting both generator set-points as well as electricity prices, flexible FCNN models are sufficient and – due to their significantly shorter training times – superior to GNN (and CNN) models with similar number of parameters.

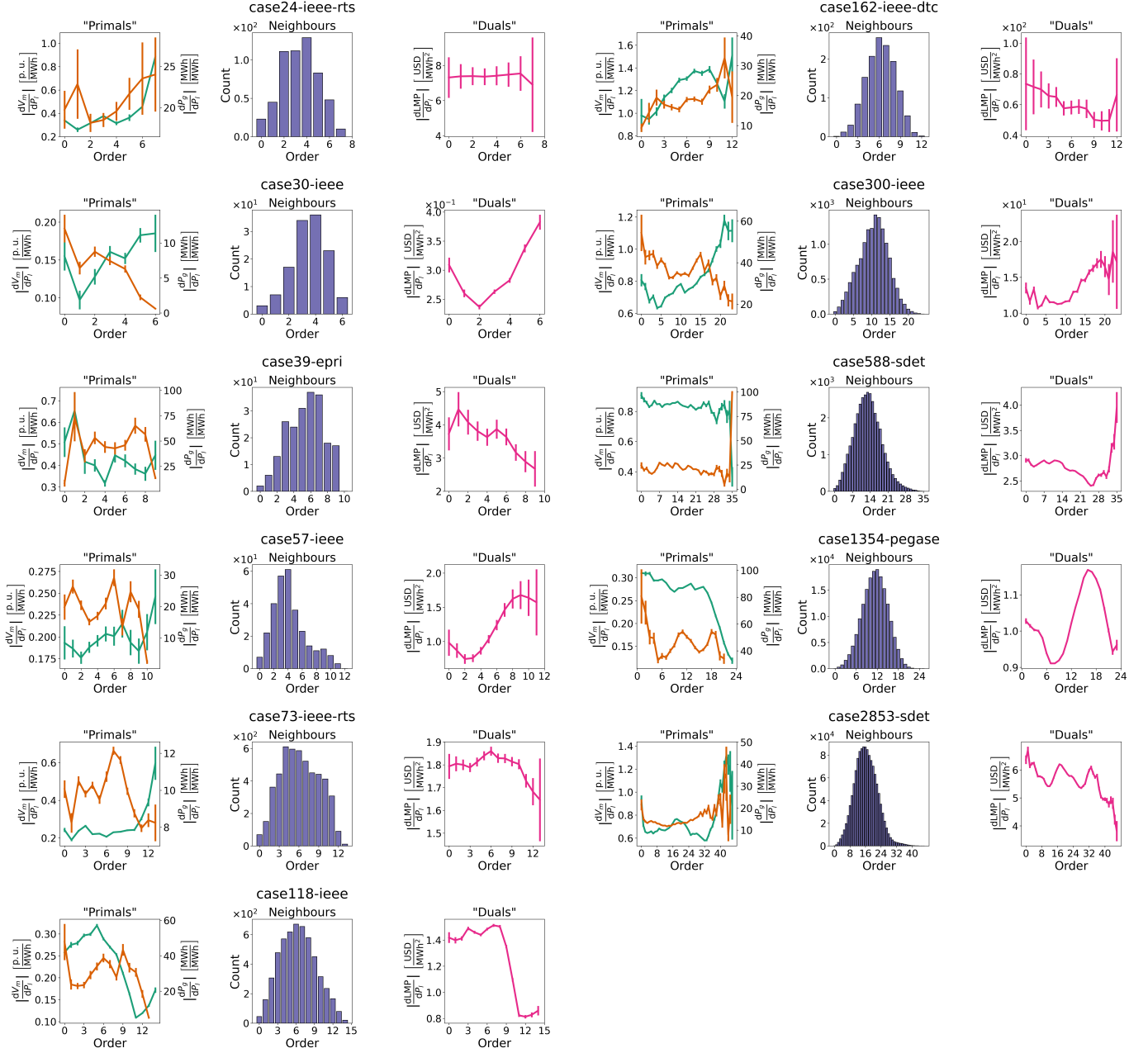


Fig. 5. Analysis of locality properties for each synthetic grid. Left and right panels show the average absolute value of the relative change (with two side 95% confidence intervals) in voltage magnitude (green), injected power (orange) and locational marginal prices (purple), respectively, as a function of the topological distance from the perturbed load. Centre panels show the distribution of generators with respect to the neighbourhood order.

REFERENCES

- [1] A. J. Wood, B. F. Wollenberg, and G. B. Sheble, *Power generation, operation, and control*. Wiley-InterScience, 2014.
- [2] A. Wachter and L. Biegler, "On the implementation of an interior-point filter line-search algorithm for large-scale nonlinear programming," *Mathematical programming*, vol. 106, pp. 25–57, 2006.
- [3] A. Castillo, C. Laird, C. A. Silva-Monroy, J. Watson, and R. P. O'Neill, "The unit commitment problem with ac optimal power flow constraints," *IEEE Transactions on Power Systems*, vol. 31, no. 6, pp. 4853–4866, 2016.
- [4] J. Rahman, C. Feng, and J. Zhang, "Machine learning-aided security constrained optimal power flow," in *IEEE Power Energy Society General Meeting (PESGM)*, 2020, pp. 1–5.
- [5] I. Mezghani, S. Misra, and D. Deka, "Stochastic ac optimal power flow: A data-driven approach," 2019.
- [6] S. H. Low, "Convex relaxation of optimal power flow—part i: Formulations and equivalence," *IEEE Transactions on Control of Network Systems*, vol. 1, no. 1, pp. 15–27, 2014.
- [7] S. Bolognani and F. Dörfler, "Fast power system analysis via implicit linearization of the power flow manifold," in *53rd Annual Allerton Conference on Communication, Control, and Computing (Allerton)*. IEEE Press, 2015, p. 402–409.
- [8] A. Bernstein and E. Dall'Anese, "Linear power-flow models in multiphase distribution networks," in *IEEE PES Innovative Smart Grid Technologies Conference Europe (ISGT-Europe)*, 2017, pp. 1–6.
- [9] M. B. Cain, R. P. O'Neill, and A. Castillo, "History of optimal power flow and formulations," *Federal Energy Regulatory Commission*, vol. 1, pp. 1–36, 2012.
- [10] A. von Meier, *Electric Power Systems: A Conceptual Introduction*. Wiley-InterScience, 2006.
- [11] K. Baker, "Solutions of dc opf are never ac feasible," 2020.

- [12] FERC, "Recent iso software enhancements and future software and modeling plans." [Online]. Available: <https://cms.ferc.gov/sites/default/files/2020-05/rto-iso-soft-2011.pdf>
- [13] A. Shahzad, E. C. Kerrigan, and G. A. Constantinides, "A warm-start interior-point method for predictive control," in *UKACC International Conference on Control*, 2010, pp. 1–6.
- [14] Q. Zhou, L. Tesfatsion, and C.-C. Liu, "Short-term congestion forecasting in wholesale power markets," *IEEE Transactions on Power Systems*, vol. 26, no. 4, pp. 2185–2196, 2011.
- [15] L. A. Roald and D. K. Molzahn, "Implied constraint satisfaction in power system optimization: The impacts of load variations," in *2019 57th Annual Allerton Conference on Communication, Control, and Computing (Allerton)*, 2019, pp. 308–315.
- [16] X. Ma, H. Song, M. Hong, J. Wan, Y. Chen, and E. Zak, "The security-constrained commitment and dispatch for midwest iso day-ahead co-optimized energy and ancillary service market," in *IEEE Power, Energy & Society General Meeting*, 2009, pp. 1–8.
- [17] Y. LeCun, Y. Bengio, and G. Hinton, "Deep learning," *Nature*, vol. 521, pp. 436–44, 2015.
- [18] N. Guha, Z. Wang, and A. Majumdar, "Machine learning for AC optimal power flow." ICML, Climate Change: How Can AI Help? Workshop, 2019.
- [19] F. Fioretto, T. W. K. Mak, and P. V. Hentenryck, "Predicting ac optimal power flows: Combining deep learning and lagrangian dual methods," 2019.
- [20] K. Baker, "Learning warm-start points for ac optimal power flow," *2019 IEEE 29th International Workshop on Machine Learning for Signal Processing (MLSP)*, pp. 1–6, 2019.
- [21] A. Robson, M. Jamei, C. Ududec, and L. Mones, "Learning an optimally reduced formulation of opf through meta-optimization," 2020.
- [22] S. Misra, L. Roald, and Y. Ng, "Learning for constrained optimization: Identifying optimal active constraint sets," 2019.
- [23] D. Deka and S. Misra, "Learning for dc-opf: Classifying active sets using neural nets," 2019.
- [24] L. Chen and J. E. Tate, "Hot-starting the ac power flow with convolutional neural networks," 2020.
- [25] D. Owerko, F. Gama, and A. Ribeiro, "Optimal power flow using graph neural networks," in *ICASSP 2020 - 2020 IEEE International Conference on Acoustics, Speech and Signal Processing (ICASSP)*, 2020, pp. 5930–5934.
- [26] T. Falconer and L. Mones, "Deep learning architectures for inference of ac-opf solutions," 2020.
- [27] T. Falconer, "Reducing the computational cost of ac optimal power flow with geometric deep learning," 2020.
- [28] L. Halilbašić, F. Thams, A. Venzke, S. Chatzivasileiadis, and P. Pinson, "Data-driven security-constrained ac-opf for operations and markets," in *2018 Power Systems Computation Conference (PSCC)*, 2018, pp. 1–7.
- [29] X. Pan, T. Zhao, M. Chen, and S. Zhang, "Deepopf: A deep neural network approach for security-constrained dc optimal power flow," 2020.
- [30] F. Zhou, J. Anderson, and S. H. Low, "The optimal power flow operator: Theory and computation," 2020.
- [31] A. Zamzam and K. Baker, "Learning optimal solutions for extremely fast ac optimal power flow," 2019.
- [32] M. Jamei, L. Mones, A. Robson, L. White, J. Requeima, and C. Ududec, "Meta-optimization of optimal power flow." ICML, Climate Change: How Can AI Help? Workshop, 2019.
- [33] University of Washington: Department of Electrical & Computer Engineering, "Power systems test case archive." [Online]. Available: <http://labs.ece.uw.edu/pstca/>
- [34] N. Dehmamy, A.-L. Barabási, and R. Yu, "Understanding the representation power of graph neural networks in learning graph topology," 2019.
- [35] J. Zhou, G. Cui, S. Hu, Z. Zhang, C. Yang, Z. Liu, L. Wang, C. Li, and M. Sun, "Graph neural networks: A review of methods and applications," 2021.
- [36] Z. Wu, S. Pan, F. Chen, G. Long, C. Zhang, and P. S. Yu, "A comprehensive survey on graph neural networks," *IEEE Transactions on Neural Networks and Learning Systems*, vol. 32, no. 1, pp. 4–24, 2021.
- [37] T. N. Kipf and M. Welling, "Semi-supervised classification with graph convolutional networks," 2017.
- [38] M. Defferrard, X. Bresson, and P. Vandergheynst, "Convolutional neural networks on graphs with fast localized spectral filtering," 2017.
- [39] C. Morris, M. Ritzert, M. Fey, W. L. Hamilton, J. E. Lenssen, G. Rattan, and M. Grohe, "Weisfeiler and leman go neural: Higher-order graph neural networks," 2020.
- [40] P. Veličković, G. Cucurull, A. Casanova, A. Romero, P. Liò, and Y. Bengio, "Graph attention networks," 2018.
- [41] M. Fey and J. E. Lenssen, "Fast graph representation learning with PyTorch Geometric," 2019.
- [42] Z. Wu, S. Pan, F. Chen, G. Long, C. Zhang, and P. S. Yu, "A comprehensive survey on graph neural networks," *IEEE Transactions on Neural Networks and Learning Systems*, vol. 32, no. 1, p. 4–24, 2021.
- [43] M. Fey, J. E. Lenssen, F. Weichert, and H. Müller, "Splinescnn: Fast geometric deep learning with continuous b-spline kernels," 2018.
- [44] S. Babaeinejadsarookolae, A. Birchfield, R. D. Christie, C. Coffrin, C. DeMarco, R. Diao, M. Ferris, S. Fliscounakis, S. Greene, R. Huang, C. Jozs, R. Korab, B. Lesieutre, J. Maeght, T. W. K. Mak, D. K. Molzahn, T. J. Overbye, P. Panciatici, B. Park, J. Snodgrass, A. Tbaileh, P. V. Hentenryck, and R. Zimmerman, "The power grid library for benchmarking ac optimal power flow algorithms," 2021.
- [45] C. Coffrin, R. Bent, K. Sundar, Y. Ng, and M. Lubin, "PowerModels.jl: An open-source framework for exploring power flow formulations," in *Power Systems Computation Conference (PSCC)*. IEEE, 2018, pp. 1–8.
- [46] J. Bezanson, S. Karpinski, V. B. Shah, and A. Edelman, "Julia: A fast dynamic language for technical computing," 2012.
- [47] D. P. Kingma and J. Ba, "Adam: A method for stochastic optimization," 2017.
- [48] S. Ioffe and C. Szegedy, "Batch normalization: Accelerating deep network training by reducing internal covariate shift," 2015.
- [49] B. Xu, N. Wang, T. Chen, and M. Li, "Empirical evaluation of rectified activations in convolutional network," 2015.
- [50] A. Paszke, S. Gross, F. Massa, A. Lerer, J. Bradbury, G. Chanan, T. Killeen, Z. Lin, N. Gimelshein, L. Antiga, A. Desmaison, A. Kopf, E. Yang, Z. DeVito, M. Raison, A. Tejani, S. Chilamkurthy, B. Steiner, L. Fang, J. Bai, and S. Chintala, "Pytorch: An imperative style, high-performance deep learning library," in *Advances in Neural Information Processing Systems 32*. Curran Associates, Inc., 2019, pp. 8024–8035.
- [51] N. G. Singhal, J. Kwon, and K. W. Hedman, "Generator contingency modeling in electric energy markets: Derivation of prices via duality theory," 2019.
- [52] S. Liu, C. Wu, and H. Zhu, "Graph neural networks for learning real-time prices in electricity market," 2021.